Thermal condition monitoring of large smart bearing through fiber optic sensors

Thermal condition monitoring of large smart bearing through fiber optic sensors

Eugenio Brusa, Matteo Dalla Vedova, Lorenzo Giorio, Paolo Maggiore

Department of Mechanical and Aerospace Engineering

and Interdepartmental Centre PhotoNext –Applied Photonics

Politecnico di Torino, Italy

Corso Duca degli Abruzzi, 24 – 10129 Torino, Italy

Email: eugenio.brusa@polito.it (corresponding author), matteo.dallavedova@polito.it, paolo.maggiore@polito.it, lorenzo.giorio@studenti.polito.it

Abstract

The 'Smart Manufacturing' applied to steelmaking includes a continuous condition monitoring of the mill system, performed by bearings equipped with sensors. They are embedded inside the mill cage, and exposed to heat sources. Monitoring their temperature is mandatory. Fibre optics sensors can be exploited. Their behaviour is here modelled, and then tested on some prototypes. The fibre optics technology looks suitable for this application, provided that a precise sensor calibration is performed. A technological assessment is required, to develop the industrial product.

Keywords

Systems engineering, Structural Health Monitoring (SHM), Structural Mechatronics, Smart Bearing, Smart Manufacturing.

1. Introduction

The implementation of 'Smart Manufacturing' [1] in steelmaking is aimed to perform the rolling mill prognosis and diagnosis, to prevent critical failures and undesired marks on the rolled product [2]. The 'smart bearing', equipped with sensors, is used like a sentry of mill operation [3]. The so–called 'in–monitoring' identifies the bearing damage and wear, while the 'out-monitoring' monitors the mill operation. The monitoring activity includes many measurement targets as vibration, load, temperature, and strip or rod speed.

The temperature is a crucial parameter, since bearings are embedded inside the mill cage, and are exposed to a severe heating, which affects the stress distribution, as in many industrial rotors [4]. The thermal control based on distributed sensors assures an effective lubrication, and preserves the bearing life. Capacitive MEMS sensors embedded in the bearing ring do not look compatible with these working conditions [5], because power feeding and communication are inhibited by some saddles (Fig.1).

FIGURE 1

The current research activity aims to design miniaturized and autonomous bearing sensors [6]. Fibre optics sensors are therefore candidate [7]. The presence of a massive pin inside the mill cage allows embedding the fibres, and thus the need for wireless sensors and autonomy vanishes, because the FBG sensors are intrinsically powered by the light source. The safety against fire and the EMC are assured, since fibres optics are shielded, based on the light detection, and electrically isolated. They provide a high bandwidth, high signal to noise ratio, multiple sensors per fibre, at a competitive cost [8]. The above mentioned needs motivates the study of optical Fibres with Bragg Grating (FBG), to design some bearing sensors to detect the temperature of rings [9]. This solution is here investigated and tested, through an experimental characterization of sensors.

2. Requirements and technology

The Fibre Bragg Grating Sensors (FBGS) are applied to the thermal monitoring of the mill cage. They must be embedded inside the central pin, and exposed to air, lubricant or water. The goal is measuring the temperature of inner ring, which is fixed, while the outer ring rotates. Measurements must be stable in time, reliable in terms of precision, repeatability, statistic relevance and sensitivity. The temperature of lubricant inside the roller bearing must not exceed 120°C, and a warning must be sent, when it reaches 70°C. The preferred measurement resolution is 0.5°C, although 1°C is accepted.

The Bragg grating is a finite region of the fibre optics, in which a periodic variation of the core refractive index is applied [10]. This variation acts as a selective mirror, which stops the transmission of light, at a specific wavelength [11]. The light is reflected, and propagates backwards to the source, within the fibre core. A spectrum analyser detects the light, as an interferometric system. The FBGS provide several advantages,

although some limitations are still present. They exhibit a very high resistance against corrosion. The signal is independent on the distance and on the intensity of light. Each fibre includes several sensors, from ten to one hundred, which are operated in parallel, and thus it is compact and allows a redundancy. The FBGS gain 700°C, because of their coating layers. The cost of interrogators is still high, but it looks compatible with that of the rolling mill. The sensor calibration is rather difficult, the radii of curvature of installed optical fibres are usually greater than 10 mm, and the sensitivity of sensors is small (Kε = 1÷1.3 nm mm/m).

3. Sensor development

The size of roller bearings for the mill cage allows creating a dedicated pit within the inner ring, where the fibre is deposed and fixed, to measure the local temperature. The wavelength reflected by the Bragg grating, λ_B, complies with so-called Bragg condition:

$$\lambda_B = 2n_{eff}\Lambda \tag{1}$$

where Λ is the grating pitch, i.e. the distance between grating targets, and n_{eff} is the effective refractive index of the propagation mode. It is similar to the refractive index, but it is evaluated for the wave propagating inside transversely limited media, as [10]:

$$n_{eff} \cong n_{cladding} + \left(1.1428 - \frac{0.996}{v}\right)^2 \Delta n \tag{2}$$

where $\Delta n = n_{core} - n_{cladding}$, and ν is a function of Δn and of the wavelength λ of light. Several agents applied to the sensor, as strain, temperature and pressure, change λ_B, and their effect is related to the peek shift in the sensor response spectrum. A typical FBGS has a length of a few millimetres, a reflected bandwidth lower than 1nm and might achieve the 100% reflection of the peak luminous intensity [12]. When the FBGS undergoes only a temperature change ΔT, the related wavelength shift $\Delta\lambda_T$ can be expressed as [1]:

$$\Delta\lambda_T = \lambda_B(\alpha_0 + \beta_0)\Delta T = K_T \Delta T \tag{3}$$

where α_0 is the thermal expansion coefficient of the fibre, β_0 is the thermo-optic coefficient and K_T is referred to as temperature sensitivity coefficient. Typical values for silica optical fibres are $\alpha_0 = 0.55 \cdot 10^{-6}$ (◦C)$^{-1}$ and $\beta_0 = 6.6 \cdot 10^{-6}$ (◦C)$^{-1}$. The linear relation of Eq.(3) is only valid within a certain range of temperature (T< 100◦C), while for higher temperatures a nonlinear formulation must be used [13]:

$$\beta_0 = \frac{1}{n_0}\frac{dn_{eff}}{dT} = 5.327\cdot10^{-6} + 9.546\cdot10^{-9}\,T - 4.173\cdot10^{-12}T^2 \quad (4)$$

Some experimental tests demonstrate Eq.(4) underestimates the real coefficients [14-15]. It is relevant that n_{eff} changes significantly with the fibre characteristics, even when changes are very small. This is a critical issue for the design, and needs to be precisely characterized.

4. Experimental set-up

To identify the temperature sensitivity coefficients, K_T, some prototypes of FBGS (properties in Table 1) were set up in a test bench including a resistance thermometer PT-100 (properties in Table 2) and a Peltier cell controlled by a Thermo-Electric Controller Meerstetter TEC-1091. The Peltier cell simulates the heating process in operation, by means of a PID (proportional–integral–derivative) controller regulating the intensity of feeding current.

TABLE 1

TABLE 2

The controller TEC–1091 calculates the Peltier command input *u(t)* as a function of the error *e(t)*:

$$u(t) = K_P\left(e(t) + \frac{1}{T_i}\int_0^t e(\tau)d\tau + T_d\frac{de(t)}{dt}\right) \quad (5)$$

where *e(t)* is the difference between the target temperature and that measured by the PT-100), K_p the proportional gain, T_i the integration time, T_d the derivative time, being defined by the user. The characteristic time of evolution of thermal behaviour motivated the selection of parameters, with T_d almost null, K_p set by the "Auto-Tuning" function available inside the TEC controller, with a mean value of K_p = 30% °C^{-1}, and T_i = 30 s to 300 s, depending on the speed required to adjust the regulation. The interrogator Smart Scan Interrogator (Smart Fibers®) performs the measurement of wavelength changes, $\Delta\lambda_B$, as temperature varies. It is able to handle four fibres simultaneously, each one with up to 16 FBG sensors installed, managed by the Wavelength Division Multiplexing Method.

To uniformly heat the FBGS, a first test bench, consisting of a pair of plates that lock a Peltier cell keeping it in contact with the optical sensor, was developed (Fig.2).

FIGURE 2

This system looks sensitive to slight changes of the tightening torque applied to bolts. The locking system does not allow the fibre expanding along its transversal direction, therefore an error might occur on the longitudinal strain, which causes a variation, $\Delta\lambda_\varepsilon$, being rather difficult to be measured. The fibres are bonded on the surface of support, through a silicon layer, sufficiently far to avoid any interference. The temperature sensed by the thermometer PT-100 and the output current of Peltier cell are both observed. The target temperature in this test bench is achieved fairly fast, but the electric current decreases, during the first ten minutes, and then it is stabilized (Fig.3).

FIGURE 3

A second layout was developed, to minimize the contact between the Peltier cell and the thermometer. In this layout the thermometer is submerged into water and placed near the fibre optic sensor. It can be noticed that in the real system submerging the fibre within the lubricant of bearings or into the water used to feed the water jets is possible. A more powerful Peltier cell was even used, with a larger heating surface (Table 3). Experiments performed with this second test bench show an improvement of the current fed by the TEC controller and of current absorption.

TABLE 3

A new structure made by additive manufacturing in thermoplastic polymer, with a melting temperature of 70÷75°C, was built up to suitably locate the FBGS inside water heated by the Peltier cell. The support is compliant and adaptable to the frame vibration. It applies even a slight damping on the fibre (Fig.4).

FIGURE 4

5. Experimental tests

To identify the temperature sensitivity coefficient of the FBGS with Polyimide coating, a first set of experimental tests was performed between 30°C and 60°C, to simulate the regular behaviour of rolling mill, and other tests were carried out at a higher temperature, close to the melting of the AM support. The TEC Software controlled the Peltier cell, with a temperature rate of 0.02°C/s, i.e. practically in steady state response.

Results are shown in Table 4. A set of ten temperature measurements was recorded by the PT-100, whose calibration was certified, and a linear regression was calculated by means of the Ordinary Least Squares Method:

$$\{\lambda_i\} = K_T\{T_i\} + a \tag{6}$$

where a is the absolute wavelength of the linear regression for a temperature of $T = 0°C$.

TABLE 4

The coefficient of determination R^2 that checks the model consistency with observed outcomes is found as:

$$R^2 = \frac{\sum_{i=1}^{n}\left(\hat{\lambda}_i - \bar{\lambda}\right)^2}{\sum_{i=1}^{n}(\lambda_i - \bar{\lambda})^2} \tag{7}$$

where λ_i are the experimental data, $\bar{\lambda}$ their mean value, and $\hat{\lambda}_i$ values estimated by the linear regression. The significance of the linear regression coefficients was evaluated as in case of experimental results affected by uncertainty, through the Monte Carlo method [16-17]. The absolute errors, represented by the standard deviation s of measured variables, were found:

$$\begin{gathered} s[\lambda_i] = 8{\cdot}10^{-4} nm \\ s[T_i] = 10^{-2} °C \end{gathered} \tag{8}$$

Exploiting those values, for each measurement series, some vectors of independent random data were created, i.e. the data were randomly picked inside the range of variation defined by the standard deviation of direct measures, and for every one the linear regression was calculated. The range of variation of coefficients K_T and a was estimated by their standard deviation and rounded:

$$\begin{gathered} s[K_T] = 10^{-5} nm/°C \\ s[a] = 10^{-3} nm \end{gathered} \tag{9}$$

i.e. it is possible evaluating the temperature sensitivity coefficient, K_T, with a precision of 4 digits, in nm/°C, and the constant a, of 2 digits. The relation between λ and T looks appreciably linear, i.e. coefficient of determination is close to one, as in [18] (Fig.5).

FIGURE 5

The temperature sensitivity coefficient detected during tests looks coherent with the theoretical values found in the literature [12], [14], [19], [20]. The small variance of results demonstrates their accuracy, in case of unloaded fibre and free thermal expansion:

$$\overline{K_T} = \frac{1}{N}\sum_{i=1}^{10} K_{Ti} = 0.01232\ nm/°C$$
$$\sigma_{KT}^2 = \frac{1}{N}\sum_{i=1}^{10}\left(K_{Ti} - \overline{K_T}\right)^2 = 3.661{\cdot}10^{-8}\left(\frac{nm}{°C}\right)^2 \quad (10)$$

A good calibration allows keeping the error for the temperature sensitivity coefficient within 5%. The thermo-optic coefficient of fibre was also calculated, starting from Eq.(3):

$$\beta_{0exp} = \frac{\overline{K_T}}{\lambda_B} - \alpha_0 = 7.32{\cdot}10^{-6} °C^{-1} \quad (11)$$

This value is larger than those reported in the literature [14], but is smaller than the experimental result described in [21]. Therefore, it seems compatible with the state-of-the-art, although it confirms the strong dependency on the fibre layout and production.

To express the temperature sensitivity as in Eq.(3), the reference Bragg wavelength was set at the value identified by the linear regression at T_0 = 30°C. This action makes every measure contributing to the definition of the reference wavelength λ_0, to be then compared, when several series of experimental measures are analysed. The reference wavelength is calculated through Eq.(6) for given temperature T_0. A first investigation identifies the uncertainty related to the reference wavelength detected by tests:

$$\lambda_0 = \lambda_0 \pm s[\lambda_0] \quad (12)$$

The rounded value of that uncertainty looks valid for all the series of experimental measures:

$$s[\lambda_0] = 1.4{\cdot}10^{-3} nm \Leftrightarrow 2{\cdot}10^{-3} nm \quad (13)$$

As is shown in Table 4, the reference wavelength λ_0 varies significantly, and a variation of 0.04 nm corresponds to a temperature difference greater than 3°C. Therefore, in addition to fixing accurately the FBGS, it is required calibrating precisely λ_0. The smallest temperature variation detected by the FBGS is related to coefficient K_T. The interrogator measures variations multiple of $\Delta\lambda_{min}$ = 0.0008 nm, corresponding to a temperature variation greater than ΔT_{min} = 0.0008 /K_T = 0.065°C, i.e. greater than the maximum precision

which can be reached with the TEC controller, equipped with the PT-100 thermometer. The error distribution shown in Fig.6, evaluated considering as exact the measures collected by the PT-100 thermometer, is characterized by a mean value, $\mu = -0.00215$°C and a variance, $\sigma = 0.2228(°C)^2$.

FIGURE 6

That standard deviation demonstrates that a difference of up to 0.5°C can exist. This difference is compatible with the requirement expressed by the manufacturer, although it seems quite large. It is true that an undesired convective flow within the water under heating might occur. By converse, even the resistance thermometer temperature can exhibit an error, which was assumed to be null.

5. Technological assessment

The experimental activity allowed defining a procedure for a suitable installation of the FBGS, with fibre slightly folded, within a pit. The Polyimide coating increases up to 350°C the temperature limit of the Acrylate coating of 150°C. Gluing the sensor is crucial, when applied to the monitored structure, since the thermal expansion affects the behaviour of feature and adhesive, and thus modifies coefficient K_T. If load and temperature are separately measured, the silicone is used to fix the unstressed fibre, while the epoxy resins are preferred when even deformation occurs. The sensor calibration operation was even assessed. It can exploit the resistance thermometer to correlate the wavelength shift of the FBGS to the temperature change, and the Peltier cell can be used to vary the temperature. The calibration starts from a quasi-static test, with a temperature rate not exceeding 0.03°C/s, and the temperature sensitivity coefficient, $K_{T,sper}$, and the reference wavelength, $\lambda_{0,sper}$, at a reference temperature T_0 are found.

Conclusion

The use of the FBGS in thermal condition monitoring of bearings for the rolling mill is analysed. They overcome some problems of accessibility to the mill cage and avoid the risk of electric short-circuit. Investigating whether a stable measurement of temperature at the inner ring, within the range 25-70°C, with a resolution of 1°C, even in presence of water, coming from water jets, is the aim of this activity. This is

strictly connected with a precise characterization of the temperature sensitivity coefficient, K_T, of the FBGS. A test bench was built up, and used to perform the task, including a Peltier cell controlled in closed-loop with a resistance thermometer. The sensor exhibits a linear behaviour, its accuracy and resolution look compatible with the application, although the performance is lower than that of a thermometer controlled by the TEC. A flexible support in polymer is required, to make stable the contact between fibre and monitored surface. Next steps require refining the arrangement of fibre within the pit. Measuring the load applied to back-up bearing is even a relevant input for diagnosis and prognosis activities.

Acknowledgment

The authors acknowledge the support from the Politecnico di Torino through the Interdepartmental Center PhotoNext.

REFERENCES

[1] E. Brusa, "Synopsis of the MBSE, Lean and Smart Manufacturing in the product and process design for an assessment of the strategy 'Industry 4.0' ", Proc. CEUR-WS.org/Vol-2248-INCOSE Italia Conference on Systems Engineering (CIISE 2018), pp.21–30.

[2] E. Brusa, "Emerging Role of the Mechatronic Design of Industrial Systems for the Material Processing Technology" in Mechatronics: Principles, Technologies and Application, Nova Publishers, New York, 2015; ISBN: 978-1-63482-801-7, pp.185–206.

[3] E. Brusa, "Development of a sentry smart bearing as a node for connectivity and monitoring of steelmaking system" Proc. 2017 IEEE ISSE – 3rd Int. Symp. on Systems Engineering, Wien, Austria − October 11-13, 2017; 10.1109/SysEng.2017.8088257.

[4] E. Brusa, E. Ossola, "Control of thermomechanical anisotropy in high speed microrotor with permanent magnet for energy conversion", Mechanics of Advanced Materials and Structures DOI: 10.1080/15376494.2018.1501522

[5] B. Holm Hansen, R. Gao, "Vibration analysis of a sensor–integrated ball bearing", J. Vib. Acoust., Trans. ASME, 122 (2000), pp.384 –392.

[6] E. Brusa, "Design of a kinematic vibration energy harvester for a smart bearing with piezoelectric/magnetic coupling", Mechanics of Advanced Materials and Structures DOI: 10.1080/15376494.2018.1508795

[7] E. Udd et al., "Fiber optic smart bearing load structure", Proc. SPIE Conf. Nondestructive evaluation of bridges and highways III, vol.3587 Newport Beach, March 1999.

[8] M. Willsch et al., "Design of fiber optical high temperature sensors for gas turbine monitoring", Proc. 20th Optical fibre sensors, Proc. of SPIE 7503, 2009, pp.75037R-1–75037R-4.

[9] S. Konforty et al., "Bearing health monitoring using optical fiber sensors", Proc. European Conf. on the Prognostic and health management Society, 2016, pp.1-7.

[10] R. Kashyap. Fiber Bragg Gratings. Optics and Photonics. Elsevier, 2nd Ed., 2010.

[11] P.C. Berri, M.D.L. Dalla Vedova, P. Maggiore and T. Scolpito, "Feasibility study of FBG-based sensors for prognostics in aerospace applications", Journal of Physics: Conf. Series, 1249(1), Nr. 012015, 2019. DOI: 10.1088/1742-6596/1249/1/012015

[12] F.T.S. Yu and S. Yin, Fiber Optic Sensors, CRC Press, 2002.

[13] W. Wang, Y. Yu, Y. Geng, X. Li, "Measurements of thermo-optic coefficient of standard single mode fiber under large temperature range", Proc. SPIE 9620, 2015 Int. Conf. Optical Instruments and Technology, August 2015.

[14] M. Ramakrishnan, G. Rajan, Y. Semenova, and G. Farrell, "Overview of fibre optic sensor technologies for strain/temperature sensing applications in composite materials", Sensors, 16(1), 2016.

[15] M. Kreuzer, "Strain measurement with fiber bragg grating sensors", HBM, 2006.

[16] N. Hirayama, Y. Sano, "Fiber bragg grating temperature sensor for practical use", ISA Transactions, 39(2):169 – 173, 2000.

[17] K. Jones, Temperature compensation of FBG strain sensors, Smart Fibres Ltd, Notes 04, 2018.

[18] E. Oromiehie, G. Rajan, G. B. Prusty, "Thermal sensitivity and relaxation of carbon fibre-foam sandwich composites with fibre optic sensors", J. Sandwich Structures & Materials, 18(5):652–664, 2016.

[19] D.A. Krohn, T. MacDougall, A. Mendez, "Fiber optic sensors: fundamentals and applications", SPIE Press, fourth ed., 2014.

[20] K. O. Hill, G. Meltz, "Fiber Bragg Grating technology fundamentals and overview", Journal of Lightwave Technology, 15(8):1263–1276, Aug 1997.

[21] G. Adamovsky, S.F. Lyuksyutov, J.R. Mackey, B.M. Floyd, U. Abeywickrema, I. Fedin, M. Rackaitis, "Peculiarities of thermo-optic coefficient under different temperature regimes in optical fibers containing fiber bragg gratings", Optics Communications, 285(5):766 – 773, 2012.

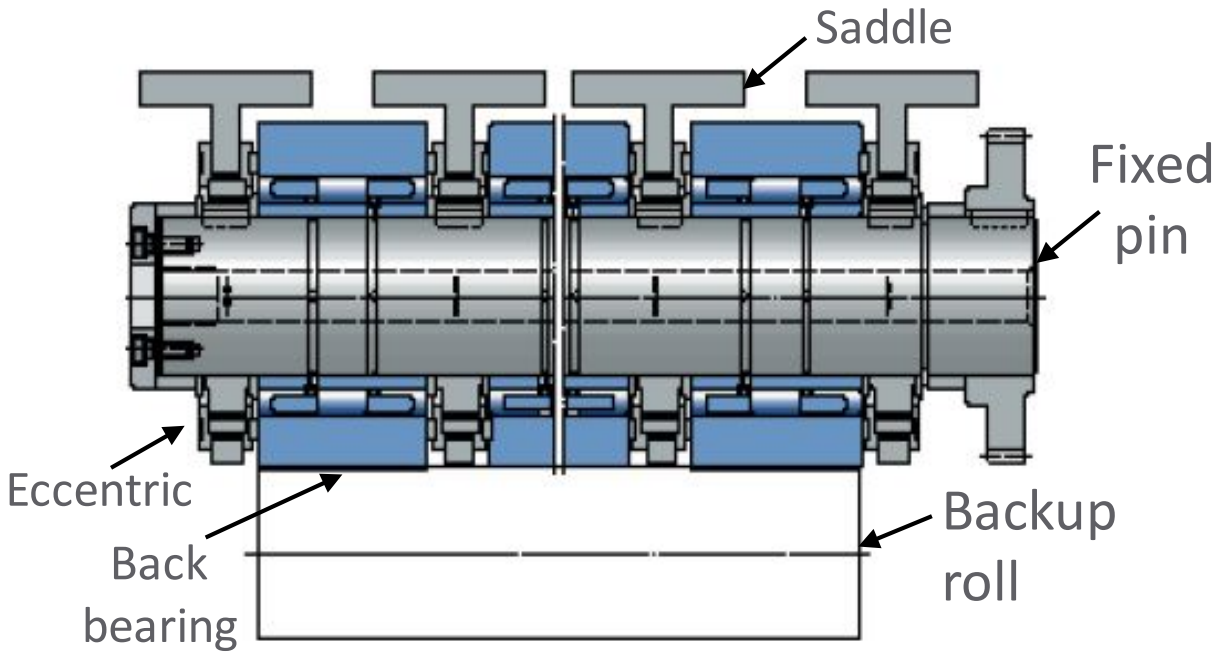

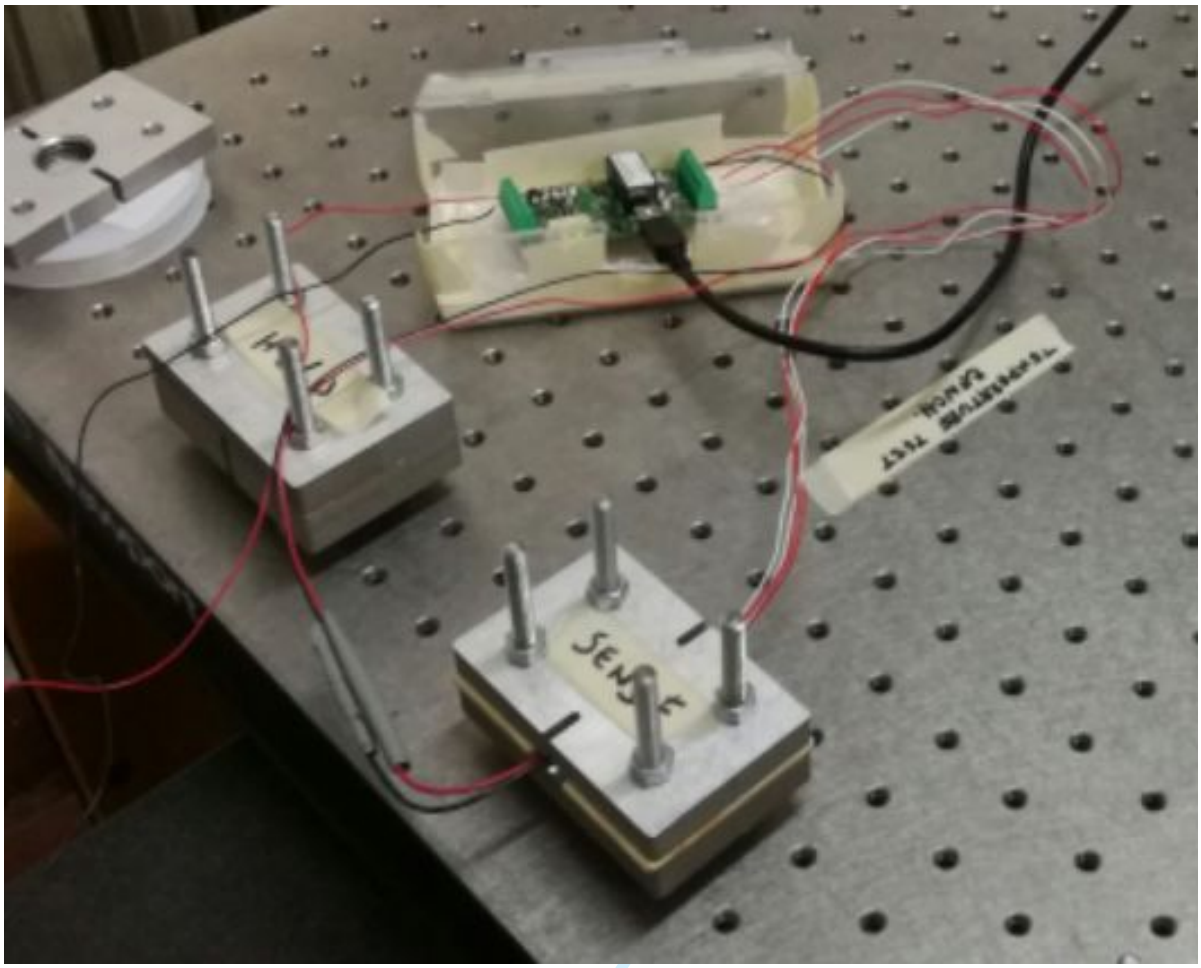

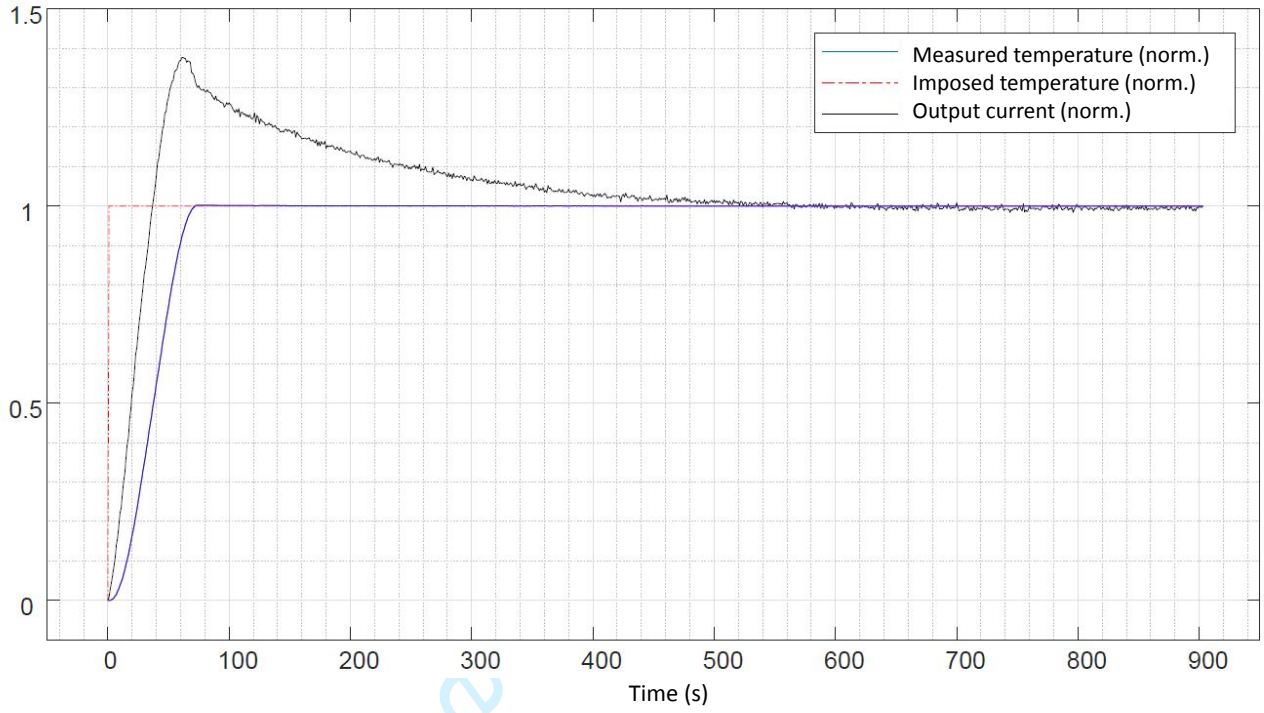

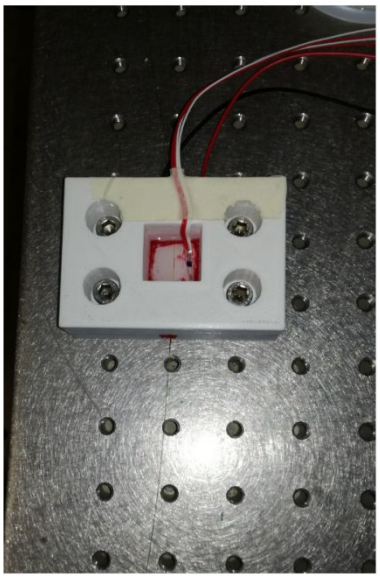

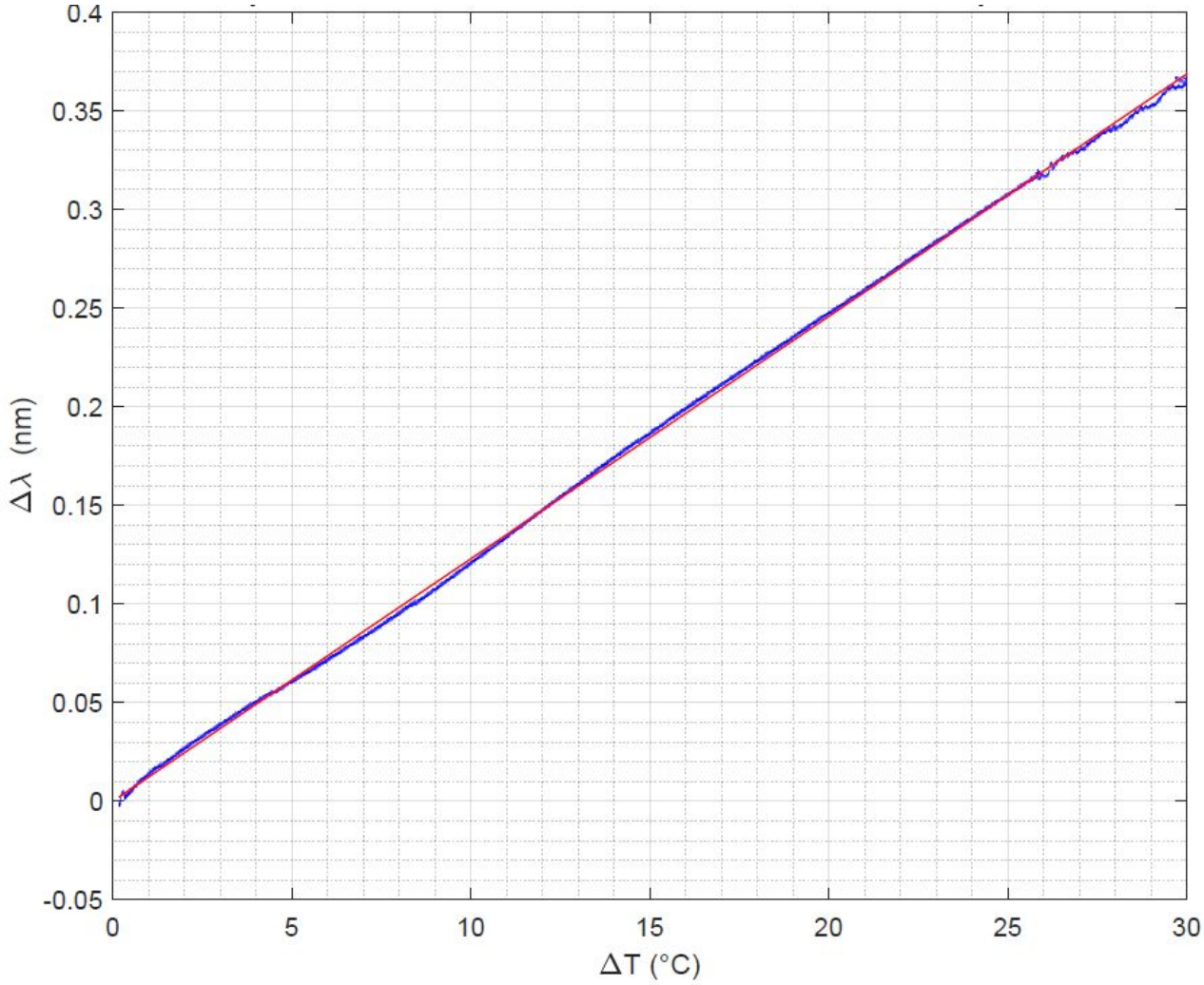

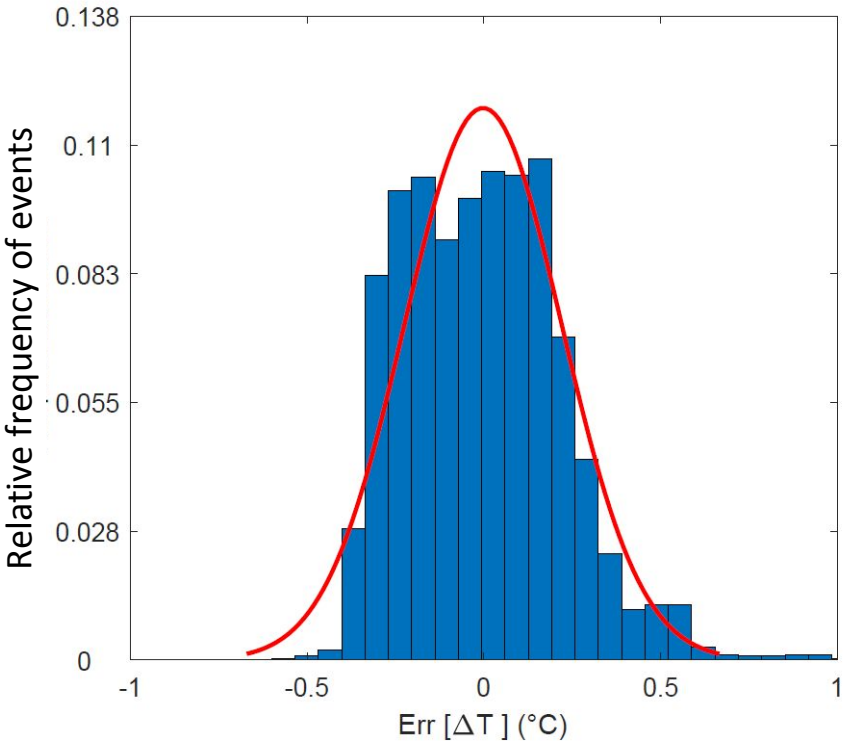

FIGURES CAPTIONS

Fig.1 Lateral view of the back bearings system with its main elements.

Fig.2 Preliminary experimental set-up for the thermal characterization of sensor performance.

Fig.3 Test about the current absorbed by the Peltier Cell in operation to reach the target temperature.

Fig.4 Experimental set-up with detail of the polymeric AM support used to locate the fibre.

Fig.5 Experimental characteristics of the FBG sensor with data and linear regression curves almost superposed.

Fig.6 Comparison between the measures of the PT-100 thermometer and the FBG sensor and error plot.

	FemtoFiberTech (B)
Manufacturer	Fibercore
Fiber type	SM1250BI
Core diameter (μm)	9.8
Cladding diameter (μm)	125
Coating	Polyimide
Central wavelength (nm)	1565.07
FBG sensor length (mm)	3.2
Reflectivity (%)	71.4
Bandwidth at $3\,dB$ (nm)	0.47
SNR, *Signal to Noise Ratio* (dB)	25.6

Sensor type	PT-100, Platinum resistance
Temperature range	-50 – +250 $^{\circ}C$
Cable configuration	4 cables
Resistance at fusion point	100 Ω
Sensor dimensions (W x L)	2 x 10 mm
Tolerance class	Class A

I_{max}	$3\ A$
V_{max}	$8.6\ V$
P_{max}	$20\ W$
ΔT_{max}	$66\ ^{\circ}C$
L x L x H	$23 \times 23 \times 3.6\ mm$
Weight	$26\ grams$

Series	$[T_{in}, T_{fin}]$ $(^{\circ}C)$	Up/Down	Measures	Meas./s	$\frac{dT}{dt}\left(\frac{^{\circ}C}{s}\right)$	$K_T\left(\frac{nm}{^{\circ}C}\right)$	a (nm)	R^2	$\lambda_0\,(30\,^{\circ}C)$ (nm)
1	[30.00, 60.00]	Up + Down	7'415	1	0.02	0.01213	1564.960	0.9995	1565.324
2	[30.00, 60.00]	Up	3'482	1	0.02	0.01228	1564.952	0.9991	1565.320
3	[25.00, 65.00]	Up	751	1	0.03	0.01207	1564.959	0.9997	1565.3205
4	[30.00, 60.00]	Up	31'584	10	0.01	0.01229	1564.957	0.9997	1565.326
5	[30.00, 60.00]	Up	31'726	10	0.02	0.01233	1564.929	0.9994	1565.296
6	[30.00, 60.00]	Up	33'881	10	0.02	0.01237	1564.922	0.9991	1565.293
7	[30.00, 60.00]	Up	28'374	10	0.02	0.01226	1564.927	0.9993	1565.294
8	[30.00, 65.00]	Up	16'374	10	0.02	0.01272	1564.913	0.9979	1565.294
9	[30.00, 65.00]	Up	14'900	10	0.02	0.01223	1564.925	0.9993	1565.292
10	[65.00, 30.00]	Down	30'535	10	0.01	0.01256	1564.923	0.9991	1565.300

TABLES CAPTIONS

Table 1: FBG sensor datasheet

Table 2: Resistance thermometer RSPro PT-100 datasheet

Table 3: Peltier cell TEC1-12706 datasheet, used for the thermal characterization of the FBG sensor.

Table 4: Collection of preliminary experimental results.

Thermal condition monitoring of large smart bearing through fiber optic sensors

Abstract

The 'Smart Manufacturing' applied to steelmaking includes a continuous condition monitoring of the mill system, performed by bearings equipped with sensors. They are embedded inside the mill cage, and exposed to heat sources. Monitoring their temperature is mandatory. Fibre optics sensors can be exploited. Their behaviour is here modelled, and then tested on some prototypes. The fibre optics technology looks suitable for this application, provided that a precise sensor calibration is performed. A technological assessment is required, to develop the industrial product.

Keywords

Systems engineering, Structural Health Monitoring (SHM), Structural Mechatronics, Smart Bearing, Smart Manufacturing.

1. Introduction

The implementation of 'Smart Manufacturing' [1] in steelmaking is aimed to perform the rolling mill prognosis and diagnosis, to prevent critical failures and undesired marks on the rolled product [2]. The 'smart bearing', equipped with sensors, is used like a sentry of mill operation [3]. The so–called 'in–monitoring' identifies the bearing damage and wear, while the 'out-monitoring' monitors the mill operation. The monitoring activity includes many measurement targets as vibration, load, temperature, and strip or rod speed. The temperature is a crucial parameter, since bearings are embedded inside the mill cage, and are exposed to a severe heating, which affects the stress distribution, as in many industrial rotors [4]. The thermal control based on distributed sensors assures an effective lubrication, and preserves the bearing life. Capacitive MEMS sensors embedded in the bearing ring do not look compatible with these working conditions [5], because power feeding and communication are inhibited by some saddles (Fig.1).

FIGURE 1

The current research activity aims to design miniaturized and autonomous bearing sensors [6]. Fibre optics sensors are therefore candidate [7]. The presence of a massive pin inside the mill cage allows embedding the fibres, and thus the need for wireless sensors and autonomy vanishes, because the FBG sensors are intrinsically powered by the light source. The safety against fire and the EMC are assured, since fibres optics are shielded, based on the light detection, and electrically isolated. They provide a high bandwidth, high signal to noise ratio, multiple sensors per fibre, at a competitive cost [8]. The above mentioned needs motivates the study of optical Fibres with Bragg Grating (FBG), to design some bearing sensors to detect the temperature of rings [9]. This solution is here investigated and tested, through an experimental characterization of sensors.

2. Requirements and technology

The Fibre Bragg Grating Sensors (FBGS) are applied to the thermal monitoring of the mill cage. They must be embedded inside the central pin, and exposed to air, lubricant or water. The goal is measuring the temperature of inner ring, which is fixed, while the outer ring rotates. Measurements must be stable in time, reliable in terms of precision, repeatability, statistic relevance and sensitivity. The temperature of lubricant inside the roller bearing must not exceed 120°C, and a warning must be sent, when it reaches 70°C. The preferred measurement resolution is 0.5°C, although 1°C is accepted.

The Bragg grating is a finite region of the fibre optics, in which a periodic variation of the core refractive index is applied [10]. This variation acts as a selective mirror, which stops the transmission of light, at a specific wavelength [11]. The light is reflected, and propagates backwards to the source, within the fibre core. A spectrum analyser detects the light, as an interferometric system. The FBGS provide several advantages, although some limitations are still present. They exhibit a very high resistance against corrosion. The signal is independent on the distance and on the intensity of light. Each fibre includes several sensors, from ten to one hundred, which are operated in parallel, and thus it is compact and allows a redundancy. The FBGS gain 700°C, because of their coating layers. The cost of interrogators is still high, but it looks compatible with that of the rolling mill. The sensor calibration is rather difficult, the radii of curvature of installed optical fibres are usually greater than 10 mm, and the sensitivity of sensors is small ($K\varepsilon = 1 \div 1.3$ nm mm/m).

3. Sensor development

The size of roller bearings for the mill cage allows creating a dedicated pit within the inner ring, where the fibre is deposed and fixed, to measure the local temperature. The wavelength reflected by the Bragg grating, λ_B, complies with so-called Bragg condition:

$$\lambda_B = 2n_{eff}\Lambda \tag{1}$$

where Λ is the grating pitch, i.e. the distance between grating targets, and n_{eff} is the effective refractive index of the propagation mode. It is similar to the refractive index, but it is evaluated for the wave propagating inside transversely limited media, as [10]:

$$n_{eff} \cong n_{cladding} + \left(1.1428 - \frac{0.996}{v}\right)^2 \Delta n \tag{2}$$

where $\Delta n = n_{core} - n_{cladding}$, and ν is a function of Δn and of the wavelength λ of light. Several agents applied to the sensor, as strain, temperature and pressure, change λ_B, and their effect is related to the peek shift in the sensor response spectrum. A typical FBGS has a length of a few millimetres, a reflected bandwidth lower than 1nm and might achieve the 100% reflection of the peak luminous intensity [12]. When the FBGS undergoes only a temperature change ΔT, the related wavelength shift $\Delta\lambda_T$ can be expressed as [1]:

$$\Delta\lambda_T = \lambda_B(\alpha_0 + \beta_0)\Delta T = K_T \Delta T \tag{3}$$

where α_0 is the thermal expansion coefficient of the fibre, β_0 is the thermo-optic coefficient and K_T is referred to as temperature sensitivity coefficient. Typical values for silica optical fibres are $\alpha_0 = 0.55 \cdot 10^{-6}$ (◦C)$^{-1}$ and $\beta_0 = 6.6 \cdot 10^{-6}$ (◦C)$^{-1}$. The linear relation of Eq.(3) is only valid within a certain range of temperature (T< 100◦C), while for higher temperatures a nonlinear formulation must be used [13]:

$$\beta_0 = \frac{1}{n_0}\frac{dn_{eff}}{dT} = 5.327 \cdot 10^{-6} + 9.546 \cdot 10^{-9}\,\mathrm{T} - 4.173 \cdot 10^{-12}\mathrm{T}^2 \tag{4}$$

Some experimental tests demonstrate Eq.(4) underestimates the real coefficients [14-15]. It is relevant that n_{eff} changes significantly with the fibre characteristics, even when changes are very small. This is a critical issue for the design, and needs to be precisely characterized.

4. Experimental set-up

To identify the temperature sensitivity coefficients, K_T, some prototypes of FBGS (properties in Table 1) were set up in a test bench including a resistance thermometer PT-100 (properties in Table 2) and a Peltier cell controlled by a Thermo-Electric Controller Meerstetter TEC-1091. The Peltier cell simulates the heating process in operation, by means of a PID (proportional–integral–derivative) controller regulating the intensity of feeding current.

TABLE 1

TABLE 2

The controller TEC–1091 calculates the Peltier command input *u(t)* as a function of the error *e(t)*:

$$u(t) = K_P\left(e(t) + \frac{1}{T_i}\int_0^t e(\tau)d\tau + T_d\frac{de(t)}{dt}\right) \quad (5)$$

where *e(t)* is the difference between the target temperature and that measured by the PT-100), K_p the proportional gain, T_i the integration time, T_d the derivative time, being defined by the user. The characteristic time of evolution of thermal behaviour motivated the selection of parameters, with T_d almost null, K_p set by the "Auto-Tuning" function available inside the TEC controller, with a mean value of K_p = 30% °C^{-1}, and T_i = 30 s to 300 s, depending on the speed required to adjust the regulation. The interrogator Smart Scan Interrogator (Smart Fibers®) performs the measurement of wavelength changes, $\Delta\lambda_B$, as temperature varies. It is able to handle four fibres simultaneously, each one with up to 16 FBG sensors installed, managed by the Wavelength Division Multiplexing Method.

To uniformly heat the FBGS, a first test bench, consisting of a pair of plates that lock a Peltier cell keeping it in contact with the optical sensor, was developed (Fig.2).

FIGURE 2

This system looks sensitive to slight changes of the tightening torque applied to bolts. The locking system does not allow the fibre expanding along its transversal direction, therefore an error might occur on the longitudinal strain, which causes a variation, $\Delta\lambda_\varepsilon$, being rather difficult to be measured. The fibres are bonded on the surface of support, through a silicon layer, sufficiently far to avoid any interference. The temperature sensed by the thermometer PT-100 and the output current of Peltier cell are both observed. The target

temperature in this test bench is achieved fairly fast, but the electric current decreases, during the first ten minutes, and then it is stabilized (Fig.3).

FIGURE 3

A second layout was developed, to minimize the contact between the Peltier cell and the thermometer. In this layout the thermometer is submerged into water and placed near the fibre optic sensor. It can be noticed that in the real system submerging the fibre within the lubricant of bearings or into the water used to feed the water jets is possible. A more powerful Peltier cell was even used, with a larger heating surface (Table 3). Experiments performed with this second test bench show an improvement of the current fed by the TEC controller and of current absorption.

TABLE 3

A new structure made by additive manufacturing in thermoplastic polymer, with a melting temperature of 70÷75°C, was built up to suitably locate the FBGS inside water heated by the Peltier cell. The support is compliant and adaptable to the frame vibration. It applies even a slight damping on the fibre (Fig.4).

FIGURE 4

5. Experimental tests

To identify the temperature sensitivity coefficient of the FBGS with Polyimide coating, a first set of experimental tests was performed between 30°C and 60°C, to simulate the regular behaviour of rolling mill, and other tests were carried out at a higher temperature, close to the melting of the AM support. The TEC Software controlled the Peltier cell, with a temperature rate of 0.02°C/s, i.e. practically in steady state response. Results are shown in Table 4. A set of ten temperature measurements was recorded by the PT-100, whose calibration was certified, and a linear regression was calculated by means of the Ordinary Least Squares Method:

$$\{\lambda_i\} = K_T\{T_i\} + a \tag{6}$$

where a is the absolute wavelength of the linear regression for a temperature of $T = 0°C$.

TABLE 4

The coefficient of determination R^2 that checks the model consistency with observed outcomes is found as:

$$R^2 = \frac{\sum_{i=1}^{n}\left(\hat{\lambda}_i - \overline{\lambda}\right)^2}{\sum_{i=1}^{n}\left(\lambda_i - \overline{\lambda}\right)^2} \tag{7}$$

where λ_i are the experimental data, $\overline{\lambda}$ their mean value, and $\hat{\lambda}_i$ values estimated by the linear regression. The significance of the linear regression coefficients was evaluated as in case of experimental results affected by uncertainty, through the Monte Carlo method [16-17]. The absolute errors, represented by the standard deviation s of measured variables, were found:

$$\begin{gathered} s[\lambda_i] = 8{\cdot}10^{-4} nm \\ s[T_i] = 10^{-2} {}^{\circ}C \end{gathered} \tag{8}$$

Exploiting those values, for each measurement series, some vectors of independent random data were created, i.e. the data were randomly picked inside the range of variation defined by the standard deviation of direct measures, and for every one the linear regression was calculated. The range of variation of coefficients K_T and a was estimated by their standard deviation and rounded:

$$\begin{gathered} s[K_T] = 10^{-5} nm/{}^{\circ}C \\ s[a] = 10^{-3} nm \end{gathered} \tag{9}$$

i.e. it is possible evaluating the temperature sensitivity coefficient, K_T, with a precision of 4 digits, in nm/°C, and the constant a, of 2 digits. The relation between λ and T looks appreciably linear, i.e. coefficient of determination is close to one, as in [18] (Fig.5).

FIGURE 5

The temperature sensitivity coefficient detected during tests looks coherent with the theoretical values found in the literature [12], [14], [19], [20]. The small variance of results demonstrates their accuracy, in case of unloaded fibre and free thermal expansion:

$$\overline{K_T} = \frac{1}{N}\sum_{i=1}^{10} K_{Ti} = 0.01232\ nm/{}^{\circ}C \tag{10}$$

$$\sigma_{KT}^2 = \frac{1}{N}\sum_{i=1}^{10}\left(K_{Ti} - \overline{K_T}\right)^2 = 3.661\cdot 10^{-8}\left(\frac{nm}{°C}\right)^2$$

A good calibration allows keeping the error for the temperature sensitivity coefficient within 5%. The thermo-optic coefficient of fibre was also calculated, starting from Eq.(3):

$$\beta_{0exp} = \frac{\overline{K_T}}{\lambda_B} - \alpha_0 = 7.32\cdot 10^{-6} °C^{-1} \quad (11)$$

This value is larger than those reported in the literature [14], but is smaller than the experimental result described in [21]. Therefore, it seems compatible with the state-of-the-art, although it confirms the strong dependency on the fibre layout and production.

To express the temperature sensitivity as in Eq.(3), the reference Bragg wavelength was set at the value identified by the linear regression at $T_0 = 30°C$. This action makes every measure contributing to the definition of the reference wavelength λ_0, to be then compared, when several series of experimental measures are analysed. The reference wavelength is calculated through Eq.(6) for given temperature T_0. A first investigation identifies the uncertainty related to the reference wavelength detected by tests:

$$\lambda_0 = \lambda_0 \pm s[\lambda_0] \quad (12)$$

The rounded value of that uncertainty looks valid for all the series of experimental measures:

$$s[\lambda_0] = 1.4\cdot 10^{-3} nm \Leftrightarrow 2\cdot 10^{-3} nm \quad (13)$$

As is shown in Table 4, the reference wavelength λ_0 varies significantly, and a variation of 0.04 nm corresponds to a temperature difference greater than 3°C. Therefore, in addition to fixing accurately the FBGS, it is required calibrating precisely λ_0. The smallest temperature variation detected by the FBGS is related to coefficient K_T. The interrogator measures variations multiple of $\Delta\lambda_{min} = 0.0008$ nm, corresponding to a temperature variation greater than $\Delta T_{min} = 0.0008 / K_T = 0.065°C$, i.e. greater than the maximum precision which can be reached with the TEC controller, equipped with the PT-100 thermometer. The error distribution shown in Fig.6, evaluated considering as exact the measures collected by the PT-100 thermometer, is characterized by a mean value, $\mu = -0.00215°C$ and a variance, $\sigma = 0.2228(°C)^2$.

FIGURE 6

That standard deviation demonstrates that a difference of up to 0.5°C can exist. This difference is compatible with the requirement expressed by the manufacturer, although it seems quite large. It is true that an undesired convective flow within the water under heating might occur. By converse, even the resistance thermometer temperature can exhibit an error, which was assumed to be null.

5. Technological assessment

The experimental activity allowed defining a procedure for a suitable installation of the FBGS, with fibre slightly folded, within a pit. The Polyimide coating increases up to 350°C the temperature limit of the Acrylate coating of 150°C. Gluing the sensor is crucial, when applied to the monitored structure, since the thermal expansion affects the behaviour of feature and adhesive, and thus modifies coefficient K_T. If load and temperature are separately measured, the silicone is used to fix the unstressed fibre, while the epoxy resins are preferred when even deformation occurs. The sensor calibration operation was even assessed. It can exploit the resistance thermometer to correlate the wavelength shift of the FBGS to the temperature change, and the Peltier cell can be used to vary the temperature. The calibration starts from a quasi-static test, with a temperature rate not exceeding 0.03°C/s, and the temperature sensitivity coefficient, $K_{T,sper}$, and the reference wavelength, $\lambda_{0,sper}$, at a reference temperature T_0 are found.

Conclusion

The use of the FBGS in thermal condition monitoring of bearings for the rolling mill is analysed. They overcome some problems of accessibility to the mill cage and avoid the risk of electric short-circuit. Investigating whether a stable measurement of temperature at the inner ring, within the range 25-70°C, with a resolution of 1°C, even in presence of water, coming from water jets, is the aim of this activity. This is strictly connected with a precise characterization of the temperature sensitivity coefficient, K_T, of the FBGS. A test bench was built up, and used to perform the task, including a Peltier cell controlled in closed-loop with a resistance thermometer. The sensor exhibits a linear behaviour, its accuracy and resolution look compatible with the application, although the performance is lower than that of a thermometer controlled by the TEC. A

flexible support in polymer is required, to make stable the contact between fibre and monitored surface. Next steps require refining the arrangement of fibre within the pit. Measuring the load applied to back-up bearing is even a relevant input for diagnosis and prognosis activities.

REFERENCES

[1] E. Brusa, "Synopsis of the MBSE, Lean and Smart Manufacturing in the product and process design for an assessment of the strategy 'Industry 4.0' ", Proc. CEUR-WS.org/Vol-2248-INCOSE Italia Conference on Systems Engineering (CIISE 2018), pp.21–30.

[2] E. Brusa, "Emerging Role of the Mechatronic Design of Industrial Systems for the Material Processing Technology" in Mechatronics: Principles, Technologies and Application, Nova Publishers, New York, 2015; ISBN: 978-1-63482-801-7, pp.185–206.

[3] E. Brusa, "Development of a sentry smart bearing as a node for connectivity and monitoring of steelmaking system" Proc. 2017 IEEE ISSE – 3rd Int. Symp. on Systems Engineering, Wien, Austria − October 11-13, 2017; 10.1109/SysEng.2017.8088257.

[4] E. Brusa, E. Ossola, "Control of thermomechanical anisotropy in high speed microrotor with permanent magnet for energy conversion", Mechanics of Advanced Materials and Structures DOI: 10.1080/15376494.2018.1501522

[5] B. Holm Hansen, R. Gao, "Vibration analysis of a sensor–integrated ball bearing", J. Vib. Acoust., Trans. ASME, 122 (2000), pp.384 –392.

[6] E. Brusa, "Design of a kinematic vibration energy harvester for a smart bearing with piezoelectric/magnetic coupling", Mechanics of Advanced Materials and Structures DOI: 10.1080/15376494.2018.1508795

[7] E. Udd et al., "Fiber optic smart bearing load structure", Proc. SPIE Conf. Nondestructive evaluation of bridges and highways III, vol.3587 Newport Beach, March 1999.

[8] M. Willsch et al., "Design of fiber optical high temperature sensors for gas turbine monitoring", Proc. 20th Optical fibre sensors, Proc. of SPIE 7503, 2009, pp.75037R-1–75037R-4.

[9] S. Konforty et al., "Bearing health monitoring using optical fiber sensors", Proc. European Conf. on the Prognostic and health management Society, 2016, pp.1-7.

[10] R. Kashyap. Fiber Bragg Gratings. Optics and Photonics. Elsevier, 2nd Ed., 2010.

[11] P.C. Berri, M.D.L. Dalla Vedova, P. Maggiore and T. Scolpito, "Feasibility study of FBG-based sensors for prognostics in aerospace applications", Journal of Physics: Conf. Series, 1249(1), Nr. 012015, 2019. DOI: 10.1088/1742-6596/1249/1/012015

[12] F.T.S. Yu and S. Yin, Fiber Optic Sensors, CRC Press, 2002.

[13] W. Wang, Y. Yu, Y. Geng, X. Li, "Measurements of thermo-optic coefficient of standard single mode fiber under large temperature range", Proc. SPIE 9620, 2015 Int. Conf. Optical Instruments and Technology, August 2015.

[14] M. Ramakrishnan, G. Rajan, Y. Semenova, and G. Farrell, "Overview of fibre optic sensor technologies for strain/temperature sensing applications in composite materials", Sensors, 16(1), 2016.

[15] M. Kreuzer, "Strain measurement with fiber bragg grating sensors", HBM, 2006.

[16] N. Hirayama, Y. Sano, "Fiber bragg grating temperature sensor for practical use", ISA Transactions, 39(2):169 – 173, 2000.

[17] K. Jones, Temperature compensation of FBG strain sensors, Smart Fibres Ltd, Notes 04, 2018.

[18] E. Oromiehie, G. Rajan, G. B. Prusty, "Thermal sensitivity and relaxation of carbon fibre-foam sandwich composites with fibre optic sensors", J. Sandwich Structures & Materials, 18(5):652–664, 2016.

[19] D.A. Krohn, T. MacDougall, A. Mendez, "Fiber optic sensors: fundamentals and applications", SPIE Press, fourth ed., 2014.

[20] K. O. Hill, G. Meltz, "Fiber Bragg Grating technology fundamentals and overview", Journal of Lightwave Technology, 15(8):1263–1276, Aug 1997.

[21] G. Adamovsky, S.F. Lyuksyutov, J.R. Mackey, B.M. Floyd, U. Abeywickrema, I. Fedin, M. Rackaitis, "Peculiarities of thermo-optic coefficient under different temperature regimes in optical fibers containing fiber bragg gratings", Optics Communications, 285(5):766 – 773, 2012.